

Magneto-optical studies of highly p -type modulation-doped GaAs/Al_xGa_{1-x}As quantum wells

S. Wongmanerod,* P. P. Paskov, P. O. Holtz, and B. Monemar

Department of Physics and Measurement Technology, Linköping University, S-581 83 Linköping, Sweden

O. Mauritz

Department of Physics, Royal Institute of Technology, S-100 44 Stockholm, Sweden

K. Reginski and M. Bugajski

Institute of Electron Technology, aleja Lotnikow 32/46, 02-668 Warsaw, Poland

(Received 19 July 2000)

We report on the optical properties of 150-Å-wide p -type modulation-doped quantum wells (QW's) with hole concentrations in the range of 0.7×10^{12} – 3.1×10^{12} cm⁻² under high applied magnetic fields up to 14 T. The magnetoexciton is clearly observed in undoped QW's, but is affected by the band mixing effect and finally quenched in the highly doped samples. The survival of the exciton up to a carrier concentration of 0.7×10^{12} cm⁻² is confirmed. The free carrier Landau level model including the valence-band mixing effect and the conduction-band nonparabolicity can nicely describe the electronic transitions in this doping regime. Moreover, the band-gap renormalization is found to be insensitive to the magnetic field variation. As a consequence, the values of interband transition energies together with the corresponding many-body shifts are accurately evaluated. Finally, an anomalous absorption feature near the Fermi edge is found to arise upon the application of high magnetic fields. This transition is proposed to be associated with a band-tail effect.

I. INTRODUCTION

The progress of epitaxial growth technology has opened the possibility to grow very-high-quality low-dimensional structures, allowing, e.g., an electron (hole) gas system with nearly perfect quasi-low-dimensional properties. This possibility has triggered numerous investigations on mainly quasi two-dimensional (2D) properties, which have resulted in many reports focused on various areas demonstrating the different properties of a two-dimensional electron or hole gas (2DEG or 2DHG). The properties of the 2D system are primarily governed by the density and type of carrier. For instance, in a system with diluted carriers, the exciton is known to form from a photoexcited electron-hole pair to dominate the radiative recombination. As the 2DEG or 2DHG density increases to a certain level, the binding energy and density of excitons are effectively reduced and the recombination is replaced by free carrier emission. Besides bleaching of the fundamental exciton, many-body interactions referred to the exchange correlation and the collective effects play a major role in the evolution of the optical spectra.¹⁻⁹ At some circumstances, e.g., upon the localization of photogenerated carriers, the formation of excitons associated with the Fermi level, the so-called Fermi-edge singularity (FES), can be simultaneously facilitated.¹⁻³ For III-V systems, such as the GaAs/AlGaAs system, it is well known that the valence-band structure is relatively complex and very different from the conduction-band structure due to the constituent interaction between the light holes (lh) and heavy holes (hh). The phenomena found in the 2DHG are considerably complicated, but in turn also more interesting from a physics point of view when compared to those of the 2DEG. The physical properties of the 2DHG have recently attracted considerable attention due to the fact that they can provide a more general understanding of fundamental physics of a 2D

system in addition to that obtained from the 2DEG cases. Recently, photoluminescence spectroscopy studies of the 2DHG have been extended into the high-density regime either in modulation-doped quantum well^{4,5} (MDQW) or in well-doped quantum well (WDQW) structures.⁶⁻⁹ In particular, novel aspects of the many-body effects such as band-gap renormalization (BGR), exciton quenching, and recombination at the Fermi edge have been investigated. Significant differences from the 2DEG case were confirmed in these studies. Moreover, the many-body calculations accounting for the valence-band mixing effect seem to agree quite well with the experimental results.

Magneto-optical measurements are realized as a useful mean to analyze low-dimensional systems. The perturbation from the magnetic field is responsible for the modification of the optical spectra due to the efficient transformation of the 2D density of state (DOS) into a 0D DOS system, which allows the optical transitions involving a specific k vector to be virtually probed by varying the field strength. However, such conditions are not only expected to unfold the optical properties of the 2DEG or 2DHG in a magnetic field but also potentially render a better understanding of the structure characteristics at zero field. Usually, the Landau level model using a single effective mass per subband is employed to undertake the interband transition problem in the presence of a magnetic field due to its simplicity and acceptable synchronism to experiments.^{10,11} In the case of wide heterostructures and quantum wells (QW's), however, the model is no longer nicely applicable, since the non-negligible effect of the valence-band nonparabolicity gives rise to an unequal-energy splitting of Landau levels. Hence the Landau level calculation accounting for the coupling between subbands (multiple-band Landau model) becomes essential.^{12,13} So far, the information on the magneto-optical properties of the 2DHG system is limited to the moderate carrier density re-

gime, where the observed optical transitions are still mixed up with a substantial contribution of excitons.¹⁴⁻¹⁷ In this work, we have proceeded with the photoluminescence (PL) spectroscopic investigations of the high-density 2DHG in wide-MDQW structures in the presence of high applied magnetic fields. The validity of the multiple-band Landau level model is tested and discussed for this high-doping regime.

II. SAMPLES AND EXPERIMENTAL SETUP

The samples used in our study are symmetric MDQW's grown by molecular-beam epitaxy. On top of a semi-insulating GaAs substrate and a GaAs buffer layer, 50 periods of 150-Å-wide undoped GaAs wells were sandwiched between 150-Å-thick Al_{0.3}Ga_{0.7}As barriers, and the structure was completed with a GaAs capping layer. In the center of each Al_xGa_{1-x}As barrier, a 50-Å-thick Be-doped layer was grown. A series of samples was prepared with varying acceptor concentration, together with an undoped reference sample. The hole sheet densities, as derived from Hall-effect measurements, are presented in Table I.

The low-temperature PL and PL excitation (PLE) measurements were carried out in an Oxford cryostat equipped with a 16-T solenoid-type superconducting magnet. The QW structure mounted with the sample plane (100) oriented perpendicularly to the magnetic field was cooled by liquid helium pumped below the λ point, so the sample temperature could be maintained below 1.8 K during the measurements. The magnetic-field-dependent measurements were arranged in the Faraday configuration. A tunable titanium-doped sapphire solid-state laser pumped by an Ar⁺ ion laser was used as an excitation light source. The laser beam was modulated using either a chopper or a photoelastic modulator prior to perpendicular focusing onto the sample. The integrated intensity of the excitation on the sample was kept below 5 W/cm². The emitted light from the samples was collected

and transmitted through a quarter-wave plate and detected by a Spex 0.85-m double-grating monochromator implemented with a cooled-GaAs photomultiplier detector. The unpolarized and circularly polarized luminescence signals were analyzed separately using the lock-in technique and the photon counting technique, respectively. For every studied sample, the PL spectra were measured with an excitation photon energy of 1.6301 eV, while PLE spectra were measured with the detection energy at the low-energy tail of the main emission peak.

III. THEORETICAL METHODS

In this section, the optical transition energies of a 150-Å-wide MDQW in the presence of a magnetic field are determined. The envelope-function formalism is employed throughout the calculations. With this approach, the motion of the hole in the structure is described by employing the four-band Luttinger Hamiltonian.^{18,19} The approach is reasonably accurate, since the split-off bands are several hundred meV below the hh and lh bands for GaAs so that the perturbation effects from the split-off band can be neglected. Under the presence of a magnetic field directed along the growth axis of the QW, the carriers possess circular motion in the plane of the QW. A suitable form of the Hamiltonian is obtained by replacing the in-plane wave vectors $k_{x,y}$ by $k_{x,y} + eA/\hbar$, where the vector potential corresponding to the Landau gauge, $\mathbf{A} = (-yB, 0, 0)$, is chosen. With the introduction of the lowering and raising operator

$$a = \sqrt{\frac{\hbar}{2eB}}(k_x - ik_y) \quad \text{and} \quad a^\dagger = \sqrt{\frac{\hbar}{2eB}}(k_x + ik_y) \quad (1)$$

together with the commutation relation $[a, a^\dagger] = 1$, the effective Hamiltonian in an arbitrary magnetic field reads

$$H_0 = - \begin{bmatrix} P+Q+\frac{3}{2}K & -S & R & 0 \\ -S^\dagger & P-Q+\frac{1}{2}K & 0 & R \\ R^\dagger & 0 & P-Q-\frac{1}{2}K & S \\ 0 & R^\dagger & S^\dagger & P+Q-\frac{3}{2}K \end{bmatrix} \begin{bmatrix} \left| \frac{3}{2}, \frac{3}{2} \right\rangle \\ \left| \frac{3}{2}, \frac{1}{2} \right\rangle \\ \left| \frac{3}{2}, -\frac{1}{2} \right\rangle \\ \left| \frac{3}{2}, -\frac{3}{2} \right\rangle \end{bmatrix}, \quad (2)$$

where

$$P = \frac{\hbar^2}{2m_0} \gamma_1 [(a^\dagger a + 1/2)s + k_z^2],$$

$$Q = \frac{\hbar^2}{2m_0} \gamma_2 [(a^\dagger a + 1/2)s - 2k_z^2],$$

$$R = \frac{\hbar^2}{2m_0} \sqrt{3} \left(-\frac{\gamma_2 + \gamma_3}{2} a^2 + \frac{\gamma_3 - \gamma_2}{2} a^{\dagger 2} \right) s,$$

$$S = \frac{\hbar^2}{2m_0} 2\sqrt{3} \gamma_3 a \sqrt{s} k_z,$$

$$K = \frac{\hbar^2}{2m_0} \kappa s.$$

TABLE I. Acceptor concentrations and estimated hole sheet concentrations.

Sample No.	N_a (cm ⁻³)	p (cm ⁻²)
Ref.	Undoped	–
193	1×10^{18}	0.7×10^{12}
194	2×10^{18}	1.3×10^{12}
195	4×10^{18}	2.2×10^{12}
196	8×10^{18}	3.1×10^{12}

γ_1 , γ_2 , γ_3 are the Luttinger parameters, κ is the hole g factor, and $s = 2eB/\hbar$.

We restrict ourselves in the present calculations to the axial approximation in which γ_2 and γ_3 in the R matrix element are set to $(\gamma_2 + \gamma_3)/2$. With this achievement the Hamiltonian is assumed to have rotational symmetry around the z axis. Accordingly, the four-component envelope function can be expressed in a separable form of

$$\Phi = \begin{bmatrix} \phi_{n-1}(x,y)f_1(z) \\ \phi_n(x,y)f_2(z) \\ \phi_{n+1}(x,y)f_3(z) \\ \phi_{n+2}(x,y)f_4(z) \end{bmatrix}, \quad (3)$$

where $\phi_n(x,y)$ are the in-plane harmonic oscillator functions satisfying the relation $a^\dagger a \phi_n = n \phi_n$ and $f(z)$ is a spin-dependent wave function along the z axis. This means that the effect of anticrossing between two levels with indices n differing by a multiple of 4 has been subsequently abandoned.

The calculations started from eigenvalues solved for zero-field conditions. The procedure is self-consistent using the standard diagonalization technique and acquiring the materials parameter specified in the work of Ekenberg *et al.*¹² Due to a very small leakage of the wave functions into the AlGaAs barrier, no difference is assumed for the Luttinger parameters and the dielectric constant between the barrier and the well materials. Using the valence-band implementation from this step, the BGR shift due to many-body interactions can be determined by the procedure ascribed in the previous work.^{5,7,9} However, we shall simply abandon this step and instead take this parameter as field independent. Subsequently, the valence-band Landau levels were computed with the initial potential profile obtained from the zero-field calculations. The redistribution of the hole wave function due to the magnetic field is taken into account by self-consistently solving the Poisson equation

$$\nabla^2 V_{sc} = \frac{e}{\epsilon_0 \epsilon_r} \left[\sum_{i \text{ occupied}} \Phi_i^\dagger \Phi_i n_i(B) + N_a(z) \right], \quad (4)$$

where V_{sc} is self-consistent potential, $N_a(z)$ is the volume density of the ionized acceptor in the AlGaAs barrier, and $n_i(B)$ is the number of holes per unit area filling the i th Landau level. The computational iterations were performed until the accuracy of the self-consistent potential was rendered below 0.3%.

Next, the conduction-band Landau level was separately calculated with inclusion of the spin splitting. The effect of

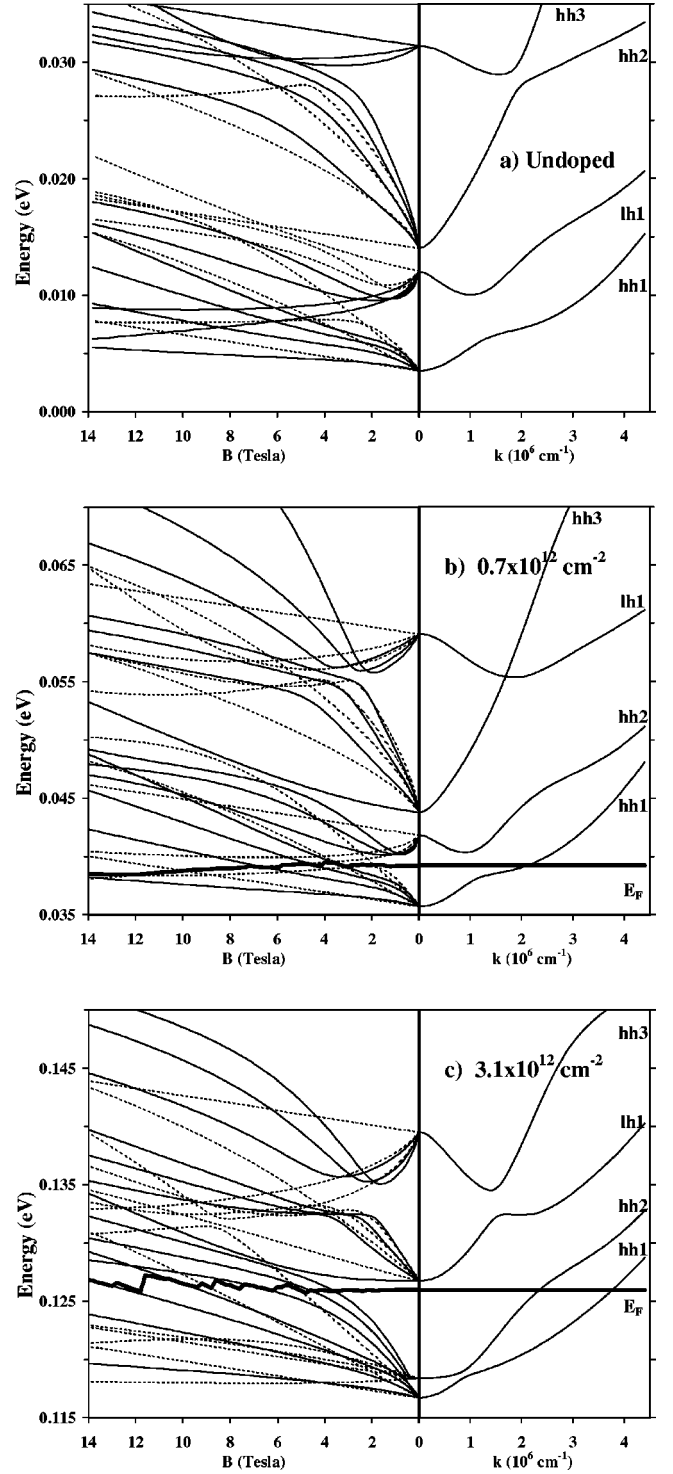


FIG. 1. Theoretical predictions for the Landau levels in the valence band (left figures) and the dispersion curves (right figures) for three different acceptor concentrations. Solid lines and dashed lines in the left figures denote spin up and spin down subbands, respectively.

the conduction-band nonparabolicity was taken into account via the correction relation $\Delta E_n(B) = K/Eg[E_n(B)]^2$. $E_n(B)$ is the n th electron Landau level measured relative to the minimum of the conduction-band profile, where the correction factor $K = -1.2$ was chosen from the work of Rogers *et al.*²⁰ Finally, the allowed Landau level transition energies between the valence band and the conduction band for dif-

ferent hole concentrations as a function of magnetic field up to 14 T were evaluated, based on the selection rule¹³ $\Delta n = \pm 1$.

For the case of undoped samples, the excitonic transition is dominant over the Landau level transitions. MacDonald and Ritchie²¹ have proposed a model, in which 2D magnetoexcitons are analyzed in two extremal regimes: (i) in the weak-field limit, where the Coulomb interaction is important. The perturbation due to the cyclotron energy gives rise to a quadratic evolution of the magnetoexciton binding energy. (ii) In the strong-field limit, where the cyclotron energy is important, the exciton behaves like free carriers with a binding energy proportional to $\approx \sqrt{B}$. In their work, in order to calculate a binding energy at an arbitrary field strength, these two extreme regimes are smoothly connected by means of the Pade' approximant. Although the model loses its sense for the interaction between excitons, the so-called exciton mixing,²² it still provides accurate values for the reduced effective mass and the effective Rydberg (binding energy). Thus, this approach in the calculations shall be adopted for the undoped structure in the following section.

In Fig. 1, the numerical results for the Landau levels at different hole concentrations with the index n limited to four hole subbands are shown and compared with the valence-band dispersion at zero field. As can be seen, a strong non-parabolic effect is clearly reflected in all cases. It is particularly obvious for the second and fourth subbands with electronlike curvature near the zone center. In the undoped structure, the second subband exhibits lh character (hence being labeled as lh1) according to its wave-function behavior at the zone center. The mass reversal effect of the lh1 is due to a strong repulsive coupling between the lh1 and hh2 via the linear k term in the off-diagonal elements of the zero-field Hamiltonian.²³ This electronlike behavior of the hole near the zone center is clearly exhibited by a reverse index ordering of linear Landau levels within the limit of weak magnetic fields (< 2 T). When the field increases above this limit, however, the Landau levels from the first and second subbands begin to approach and repel each other, resulting in an anticrossing behavior between each couple of Landau states and a redirection of most Landau levels into a holelike manner at high fields. This is analogous to the zero-field dispersion far away from the zone center (at approximately $1 \times 10^6 \text{ cm}^{-1}$), where the lh1 begins to repel the hh1 (also hh2 and hh3) via the quadratic k term in the off-diagonal element in the Hamiltonian and finally retain the holelike curvature. By gradually adjusting the acceptor density, holes become spatially separated by introducing the electrostatic field. The localization of the hole wave functions near the interfaces gives rise to the hh2 level being gradually pushed towards the hh1 as well as an increasing zone-center effective mass. We find that, as the doping level exceeds $6.5 \times 10^{17} \text{ cm}^{-3}$ (just below our doping regime), the ordering between the second and third subbands is interchanged, giving rise to a sharp reduction and increase of the lh1 and hh2 zone-center effective mass, respectively.

IV. EXPERIMENTAL RESULTS AND DISCUSSION

A. Undoped sample

The unpolarized PL and PLE spectra of the undoped sample are shown in Fig. 2(a). The fan plots of $\sigma+$ and

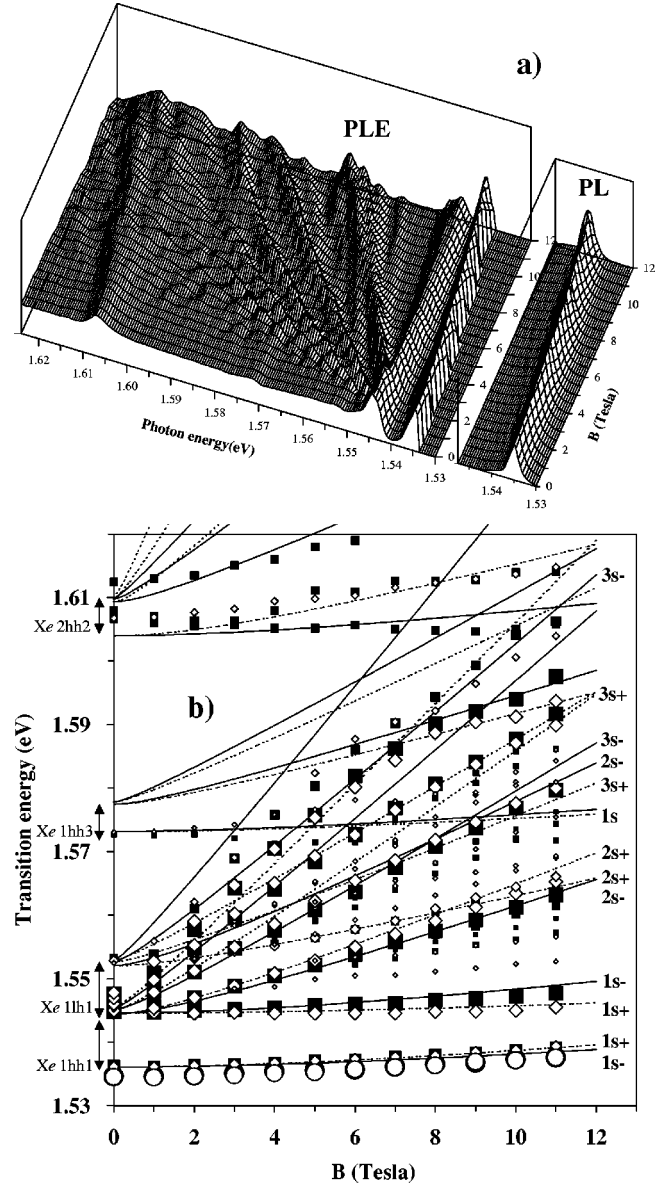


FIG. 2. (a) The low-temperature unpolarized PL and PLE spectra for the undoped sample in a varying magnetic field strength. (b) Fan diagram with the peaks extracted from the polarization-dependent PL (circles) and PLE (squares) spectra shown in comparison with the theoretically generated results for the $\sigma+$ (dashed lines) and $\sigma-$ (solid lines) polarization states with input parameters given in Table II.

$\sigma-$ components extracted from the polarization-dependent measurements are depicted in Fig. 2(b). At zero magnetic field, the observed PL peak with a linewidth of about 2 meV is interpreted as the recombination related to the transition between the ground state electron and hole ($Xe1hh1$). Indeed, this main emission is of excitonic origin, as is evident by the nonlinear blueshift behavior when increasing the magnetic field, with a measurable quadratic shift rate of $26 \mu\text{eV/T}^2$. This exciton line is also observed in the PLE spectra monitoring the low-energy tail of the PL peak with a Stoke shift smaller than 1.3 meV. The excitation spectra are dominated by the onset of the sharp enhancement of the ground-state exciton associated with the different subbands such as $Xe1lh$, $Xe1hh3$, $Xe2hh2$, etc. Furthermore, the

TABLE II. Excitons parameters for the undoped 150 Å QW's.

Exciton	Subband position (eV)	Binding energy (meV)	Exciton reduced effective masses for $\sigma+$ / $\sigma-$
<i>Xe1hh1</i>	1.545	9.2	0.070/0.062
<i>Xe1lh1</i>	1.553	8.4	0.102/0.050
<i>Xe1hh3</i>	1.577	6.4	0.340/0.065
<i>Xe2hh2</i>	1.611	6.0	0.040/0.065

excited $2s$ exciton states can be weakly observed about 7–9 meV above the corresponding ground-state peaks, denoted with arrows in Fig. 2(b), e.g., 1.547 eV for *Xe1hh1* and 1.553 eV for *Xe1lh1*. With increasing magnetic fields (within the moderate regime), the ground-state excitons in PLE spectra exhibit a quadratic blueshift similar to the one in PL, while the broad excitation parts split into a series of interband Landau-like levels and are typically denoted as $2s$, $3s$, etc. The overlapping between Landau fans from different subbands makes the Landau levels with higher index less pronounced. Nevertheless, higher states up to $6s$ are clearly revealed for *Xe1hh1*. At higher fields, where the energy levels are even better resolved, it becomes obvious that each level undergoes a Zeeman splitting into two essentially circularly polarized states with approximately equal oscillator strength [see the polarization-dependent measurement depicted in Fig. 2(b)]. For *Xe1lh1*($1s$), it is obvious that the size of splitting is negative, rather nonlinear and considered large (i.e., measures up to 3.5 meV at 12 T) when compared with *Xe1hh1*($1s$). Our observation is consistent with the work of Timofeev *et al.*²⁴ in which the anomalous splitting of these ground-state excitons was described in terms of a mixing between $1s$ (*Xe1lh1*) and $3d$ (*Xe1hh1*) states, following the theoretical predictions based on the mixing of magnetoexcitons.²² However, our experimental data can alternatively be interpreted by the model mentioned in the previous section by representing different reduced-effective-mass values for excitons with different polarizations. Figure 2(b) shows that the experimental results are nicely reproduced by the accurate values of binding energy, reduced effective mass, and the corresponding band-to-band energies as presented in Table II. Note the clearly seen anticrossing between the *Xe1hh1* and *Xe1lh1* Landau level transitions. This is useful input information for fitting of the *Xe1lh1* covering the states up to $4s$, since these transitions are associated with a weak oscillator strength. It should also be pointed out that the obtained large difference for the reduced effective masses of the $\sigma+$ and $\sigma-$ components of *Xe1lh1* is consistent with the large energy difference between the spin up and down Landau levels seen in Fig. 1(a).

B. Modulation-doped samples

The effect caused by the introduction of an increasing hole density on the optical properties of MDQW's is shown in Fig. 3. In the zero-field PL spectra for all doped samples, a strong emission peak, similar to what is seen in undoped structures, is observed together with additional features on the low-energy side. An increase in the acceptor concentration gives rise to a progressive redshift of the main emission (denoted as A) together with an asymmetric broadening. Par-

ticularly in highly doped samples, another sharp and well-defined recombination peak, labeled B, is seen on the high-energy side of the main PL peak, where the Fermi edge is expected. This peak is more pronounced with a $\sigma-$ polarization and is interpreted to be of lh character. The zero-field aspects have recently been experimentally and theoretically ascribed to many-body effects.^{4,5} The exchange-correlation effect enhances the shrinkage of the effective band gap, the so-called band-gap renormalization, resulting in a redshift of the main PL peak and a broadening of the energy levels in the so-called band-tail effect. By this implement, the new lh-related feature peak B has been interpreted as the recombination between electrons in the lowest conduction band and holes populating the lh1 band tail.

In the presence of a magnetic field up to 14 T, the main PL for the doped samples exhibits linear blueshifts with a slight broadening but no Landau level splitting can be resolved for the doping levels investigated. From the observed linear shift rate of the main PL emission of 0.86 ± 0.05 meV/T, a reduced effective mass of 0.0673 ± 0.0035 can be evaluated. Such a remarkable difference from what is observed for the undoped sample is indicative of a free carrier transition as being responsible for the emission processes, while the quenching of the hh1-related exciton occurs at slightly lower doping levels than studied here. The so-obtained reduced-effective-mass value is accordingly significantly larger than the theoretically predicted value near the GaAs band edge (0.058). This deviation implies a flattening of the hh1 subband, which is essentially due to the effect of valance-band mixing, nonparabolicity of the conduction band, and probably also the exchange-correlation effect. Thus, it is constructive to take these effects into consideration in order to analyze the structures accurately. The emission peak B is found to shift with an increasing magnetic field at a constant rate of about 0.60 meV/T and to progressively disappear in the vicinity of an applied field of 3–4 T. On the low-energy side of the main PL, three additional features are observed below the band gap (peaks C, D, and E in Fig. 3) in the presence of an applied magnetic field, with identical patterns for different samples. Moreover, they display an obvious dependence on the acceptor concentration which concerns the energy position and intensity with respect to the main PL (especially for peak C). This behavior, combined with the linear shift in a magnetic field with a rate of about 0.65–0.70 meV/T, slightly smaller than that of the main PL and PL peak energy downshifted by 14–23 meV from the main PL, suggests that the emission peaks are due to the recombination between electrons in the conduction band or bound at residual donor and holes bound at Be acceptors from different regions in the QW's structure.²⁵

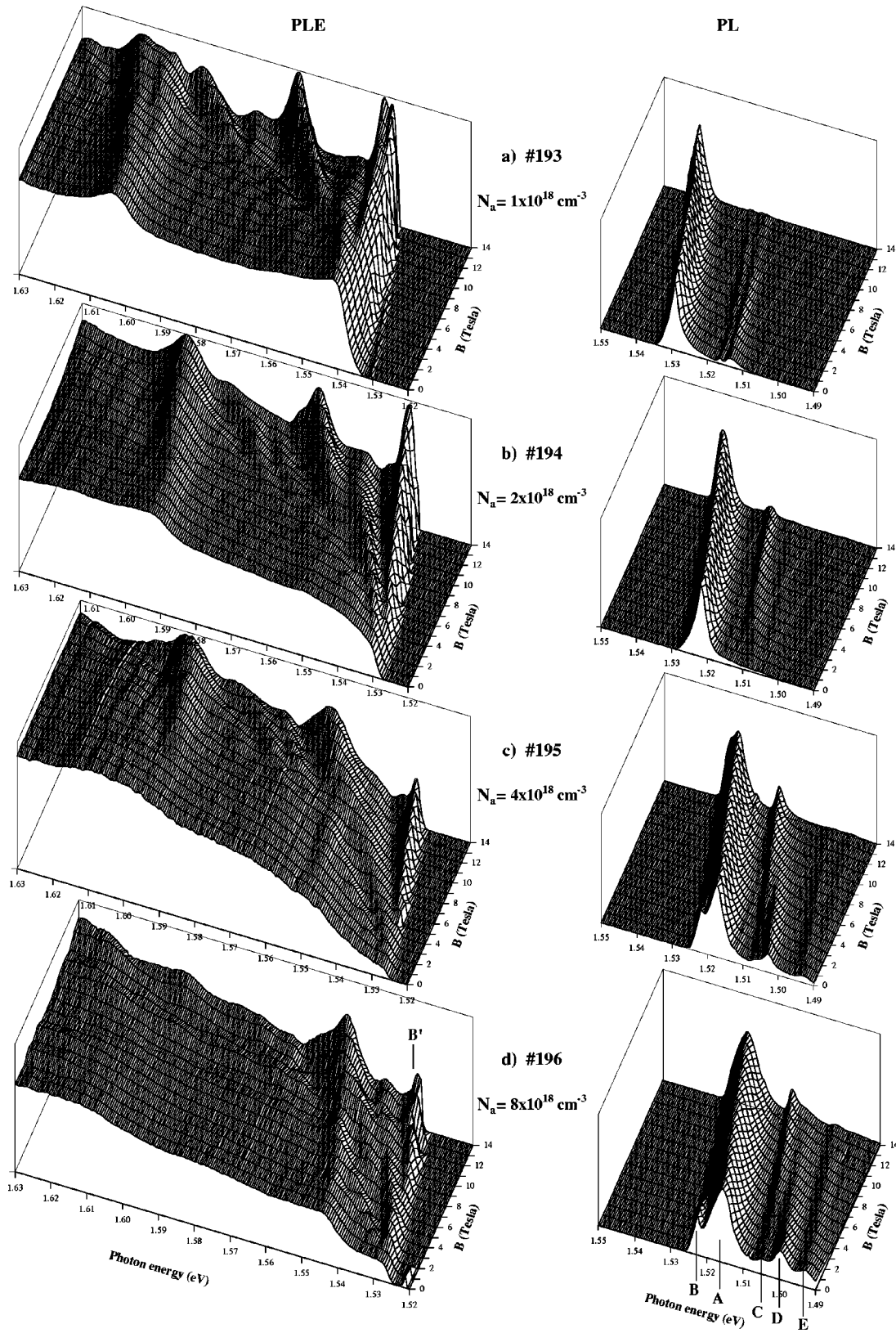


FIG. 3. The low-temperature unpolarized PL and PLE spectra for the doped MDQW samples displayed as a function of the applied magnetic field for different acceptor concentrations.

We next consider the unpolarized PLE spectra of the doped samples in Fig. 3. The zero-field PLE spectra are rather featureless and all sharp excitonic structures observed in the undoped sample are smeared out and only weakly seen in sample 193 and 194. All spectra are dominated by a

steplike absorption band. In the presence of a sufficiently high magnetic field (>5 T in sample 193), the evolution of the broad PLE band breaking into a series of more well-defined features, attributed to interband transitions between Landau levels in the conduction band and the valence band,

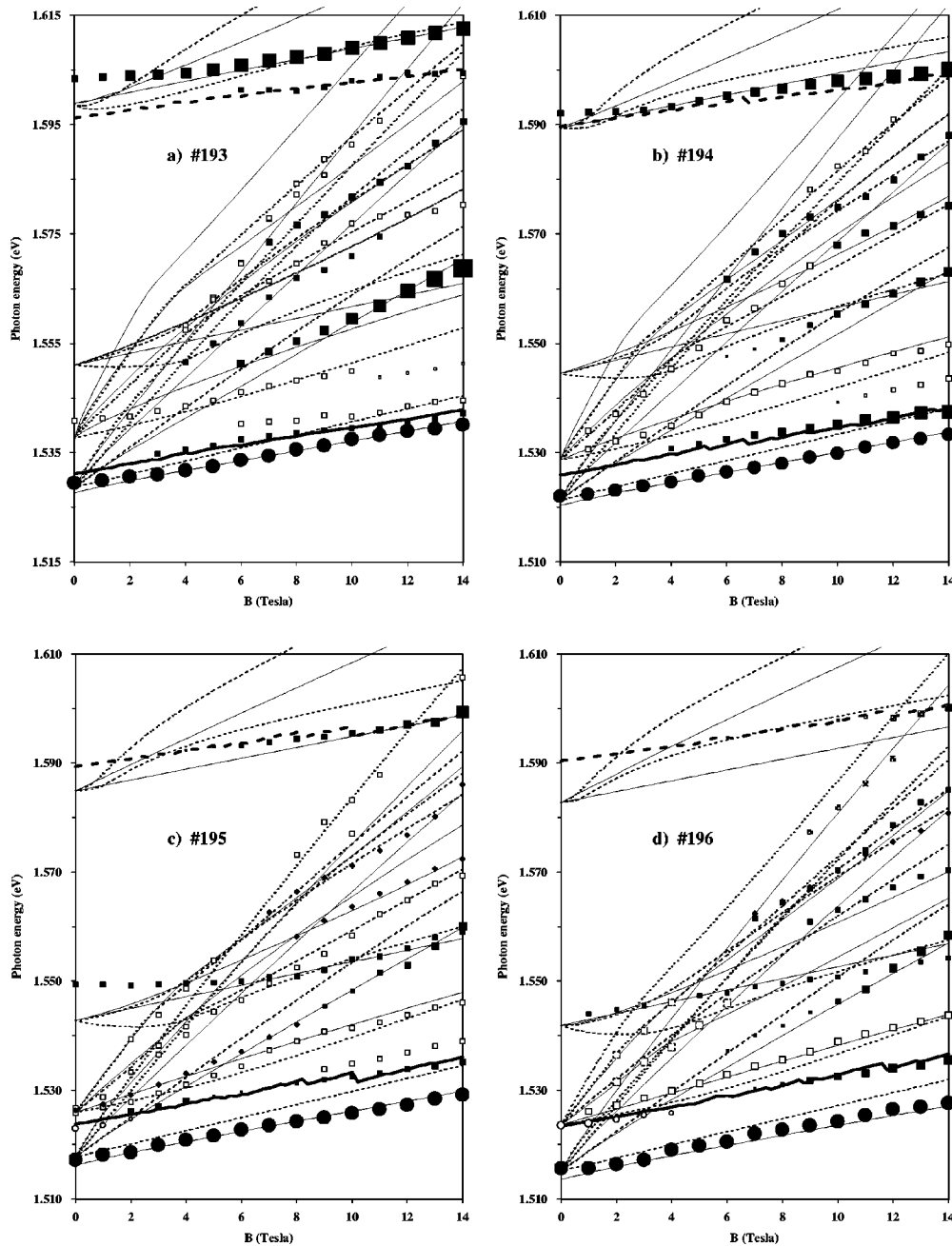


FIG. 4. The polarization-dependent Landau level transitions for different acceptor concentrations under the same measurement conditions as shown in Fig. 3. Circular and square marks represent the peaks from PL and PLE spectra, respectively. Solid and open markers show their $\sigma+$ and $\sigma-$ polarization properties, respectively. Thin solid lines and dashed lines represent the theoretically generated results for the $\sigma+$ and $\sigma-$ polarization states, respectively.

becomes discernible. However, the appearance of these features is perturbed by the increasing hole concentration as we can see from relatively fewer and broader Landau levels at higher hole density. The main mechanisms behind this variation are many-body level broadening and phase-space filling. The level broadening makes it difficult to resolve the transitions between high-index Landau levels, while the filling effect prohibits monitoring that part of the Landau level which is populated in the spectra. In particular, the low-field $e1hh1$ and $e2hh2$ transitions are seen to suffer from this effect. In all doped samples, one also finds a marked feature (labeled as B') superimposed on the absorption edge. The absorption peak B' displays a significant dependence on the acceptor

density and magnetic field which concerns both the oscillator strength and energy position. Moreover, a smooth increment of the oscillator strength together with a blueshift with a constant rate of about 0.60 meV/T is seen in all cases.

In Fig. 4, the maxima of each transition as evaluated from different polarization components in PL and PLE are presented as a function of the magnetic field. The size of each marker correlates with the strength of the transition. The theoretically generated results of allowed transitions, based on the free carrier model according to the method described above, are superimposed for comparison in the same figure. In every sample, a nearly perfect agreement between the calculated and experimental results is achieved for most of the

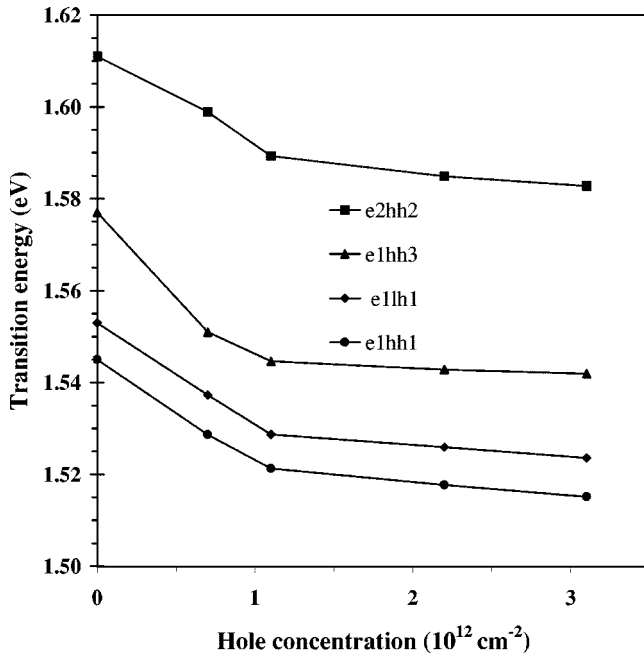


FIG. 5. Interband transition energies for the modulation-doped samples at different hole densities.

transitions, in particular for the PL peaks provided that the correction due to the conduction-band nonparabolicity is incorporated. This enables us to identify most of the transitions by their predominant character. Consequently, this indicates that the free carrier Landau level transition model is successfully applicable in this doping regime despite minor discrepancies found in the low-field regime of the low-doped sample. The reason for this discrepancy is, in principle, due to the existence of excitons as confirmed by the observed diamagnetic shift of $e1lh1$ and $e2hh2$. At higher doping, these excitons become quenched and also the second subband begins to be populated. This is consistent with our earlier reported conclusion that the exciton can survive up to an acceptor density of $4 \times 10^{18} \text{ cm}^{-3}$ according to the investigation of the zero-field PLE spectra.⁵ Moreover, it is clearly seen that there is no simple linear relationship between the energy shifts of the peaks and the magnetic field as seen in the narrow wells. This complicated picture arises from the effect of band mixing, in which the complexity is due to the proximity of the adjacent bands. Therefore, the conventional way of extrapolating the high-field data to the zero-field axis may not be an accurate method to determine transition energies in this wide-well structure, as can be seen from, e.g., the $e1hh1$ and $e1hh3$ transitions. In Fig. 5, we present accurate values of the subband positions obtained from the adjustable parameters described above. This provides the possibility to study the dimension of the BGR shift in different subbands from the lowering of these energies as a function of the hole density. The slight difference between these transitions is related to the characteristics and the occupation of holes in the related subbands. This was partly discussed in our earlier work⁵ where a good agreement with our calculations was found.

Regarding the $e2hh2$ transition in particular for all doped structures, the theoretically predicted band-to-band energies could not be well fitted to the experimental results due to a

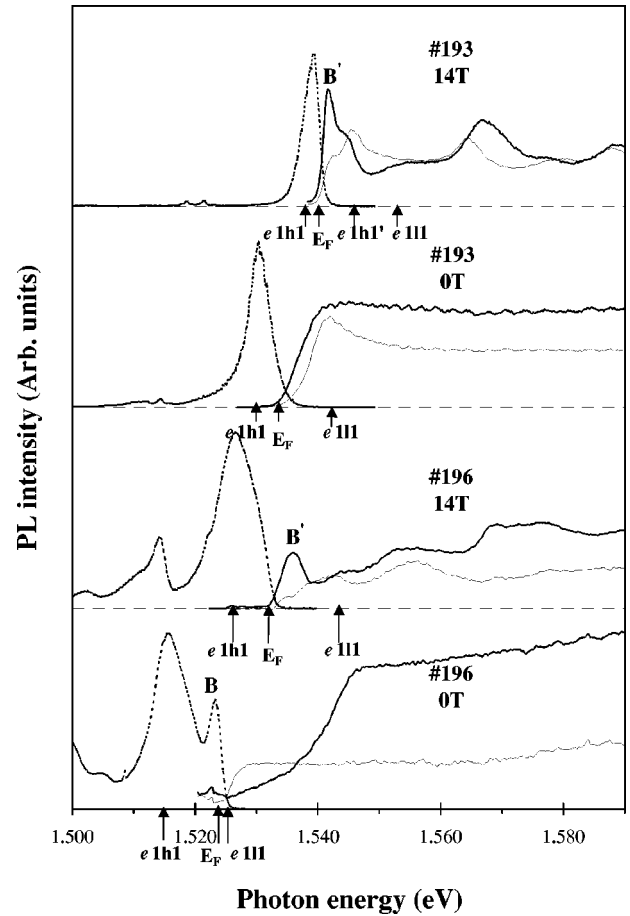


FIG. 6. Overlapping PL and PLE spectra indicating the expected position of the Fermi edge relative to the $lh1$ - and $lh1$ -related transition energies at 0 T and 14 T for samples 193 and 196.

more limited slope than theoretically predicted. A similar behavior has been reported by Kemerink *et al.*¹⁶ in which an exciton model was instead proposed. However, such an excitonic model is only applicable to our low-doped sample, 193, as mentioned above. For the samples with higher doping (194–196), the exciton oscillator strength and binding energy are reduced dramatically by several effects, e.g., phase-space filling and short-range exchange interaction.²⁷ Combining these facts, together with the calculation results in which the occupation of the second hole subband is initiated already for sample 194, the above inconsistency is more likely due to a collective effect than originating from an excitonic effect. Accordingly, the observed peak is actually a broadened $e2hh2$ transition, being partially restricted to the empty states above the Fermi sea. This is confirmed by the achieved agreement for the transition shift rate between the theoretically generated data taking the phase-space filling into account (thick dashed lines in Fig. 4) and the experimental peak trends.

We next focus on the interpretation of peak B', the $\sigma+$ polarized feature developing at the edge of the PLE spectra for every doped sample. Such an anomalous feature is usually observed in wide MDQW's as was reported elsewhere.^{10,14,26} One may assign this peak to the transition associated with another Zeeman component of the $lh1$ magnetoexciton but the g value evaluated from the corresponding Zeeman splitting is unrealistically large for these highly

doped samples. On the other hand, the magnetoexciton does not survive in these highly doped samples which means that this interpretation can be ruled out. Attempts have been made to explain a similar anomalous feature in terms of forbidden transitions between the lowest electron and the upper empty hole band Landau levels.¹⁴ On the basis of our calculations, such an interpretation is possible only for low-doped samples, while the linear shift rate of the observed peak B' is much larger than the predicted values in highly doped structures. Indeed, there is a noticeable correlation what concerns the variation of the peak intensity and position for peaks B and B' at different magnetic fields. Both peaks behave in quantitative agreement with a transition between a ground-state electron and a hole at the Fermi level (see thick solid lines in Fig. 4). The interpretation of the peak as the FES (Refs. 1–3) is unlikely in our case for several reasons stated earlier.⁵ Alternatively, the similar behavior of peaks B and B' suggests that the transitions are of the same origin, a band-tail-related transition. While peak B arises from a transition between the electron ground state in the conduction band and the occupied states of the 1lh band tail, peak B' originates from the transition between the ground-state electron and the empty states of the 1hh band tail. On the other hand, both the effects of the level broadening and the proximity between the Fermi level and the corresponding band edge play an important role on the appearances of the band-tail transitions, as illustrated in Fig. 6. In the low-doped sample, the Fermi level becomes closer to the occupied hh1 at higher fields and hence the band-tail transition appears with $\sigma+$ polarization with a rather strong intensity in PLE at high fields. Conversely, the Fermi level in the highly doped

case is very close to the empty lh1 and hence the band-tail transition appears as a $\sigma-$ peak in PL at low fields.

V. CONCLUSIONS

We have studied the 2DHG in 150-Å-wide modulation-doped quantum wells with hole concentration in the range of 0.7×10^{12} – 3.1×10^{12} cm⁻² in comparison with undoped reference QW's, under high applied magnetic fields up to 14 T. In the magneto-optical investigations, the magnetoexciton is clearly observed in the undoped QW's, but is complicated by the band mixing effect and finally quenched as the doping level increases. The survival of the excitons up to doping levels above 1×10^{18} cm⁻², corresponding to a hole sheet concentration of 0.7×10^{12} cm⁻², is confirmed. In the theoretical investigations, the free carrier Landau level model including the valence-band mixing effect and the conduction-band nonparabolicity is nicely applicable to describe the electronic transitions in this doping regime. Moreover, the BGR, a many-body effect, is found to be insensitive to magnetic field variations. As a consequence, the values of interband transition energies together with the corresponding many-body shifts are accurately evaluated. Finally, an anomalous absorption feature near the Fermi edge is found to arise by application of a high magnetic field. A transition associated with the band-tail effect is proposed.

ACKNOWLEDGMENT

S.W. gratefully acknowledges financial support from the Ministry of University Affairs, Thailand.

*Permanent address: Department of Physics, Faculty of Science, Chulalongkorn University, Thailand 10330.

¹M. S. Skolnick, J. M. Rorison, K. J. Nash, D. J. Mowbray, P. R. Tapster, S. J. Bass, and A. D. Pitt, *Phys. Rev. Lett.* **58**, 2130 (1987).

²W. Chen, H. Fritze, A. V. Nurmikko, D. Ackley, C. Colvard, and H. Lee, *Phys. Rev. Lett.* **64**, 2434 (1990).

³W. Chen, M. Fritze, W. Walecki, A. V. Nurmikko, D. Ackley, J. M. Hong, and L. L. Chang, *Phys. Rev. B* **45**, 8464 (1992).

⁴S. Wongmanerod, P. O. Holtz, K. Reginski, M. Bugajski, and B. Monemar, *Phys. Scr.* **T79**, 120 (1999).

⁵S. Wongmanerod, B. E. Sernelius, P. O. Holtz, B. Monemar, O. Mauritz, K. Reginski, and M. Bugajski, *Phys. Rev. B* **61**, 2794 (2000).

⁶A. V. Buyanov, A. C. Ferreira, E. Soderstrom, I. A. Buyanova, P. O. Holtz, B. E. Sernelius, B. Monemar, M. Sundaram, K. Campman, J. L. Merz, and A. C. Gossard, *Phys. Rev. B* **53**, 1357 (1996).

⁷A. C. Ferreira, P. O. Holtz, B. E. Sernelius, I. A. Buyanova, B. Monemar, O. Mauritz, U. Ekenberg, M. Sundaram, K. Campman, J. L. Merz, and A. C. Gossard, *Phys. Rev. B* **54**, 16 989 (1996).

⁸A. C. Ferreira, P. O. Holtz, I. A. Buyanova, B. Monemar, M. Sundaram, J. L. Merz, and A. C. Gossard, *Thin Solid Films* **306**, 244 (1997).

⁹P. O. Holtz, A. C. Ferreira, B. E. Sernelius, A. Buyanov, B.

Monemar, O. Mauritz, U. Ekenberg, M. Sundaram, K. Campman, J. L. Merz, and A. C. Gossard, *Phys. Rev. B* **58**, 4624 (1998).

¹⁰A. S. Plaut, R. T. Harley, S. R. Andrews, and T. M. Kerr, *Phys. Rev. B* **42**, 1332 (1990).

¹¹M. Potemski, J. C. Mann, K. Ploog, and G. Weimann, *Surf. Sci.* **229**, 380 (1990).

¹²U. Ekenberg and M. Altarelli, *Phys. Rev. B* **32**, 3712 (1985).

¹³J. C. Maan, A. Fasolino, G. Belle, M. Altarelli, and K. Ploog, in *Proceedings of the 17th International Conference on the Physics of Semiconductors*, edited by J. D. Chadi and W. A. Harrison (Springer-Verlag, New York, 1985), p. 463.

¹⁴L. Gravier, M. Potemski, A. Fisher, and K. Ploog, *Solid-State Electron.* **40**, 697 (1996).

¹⁵C. M. Townsley, A. Usher, B. L. Gallagher, M. Henini, and G. Hill, *Physica E* **1**, 116 (1997).

¹⁶M. Kemerink, P. M. Koenraad, P. C. M. Christianen, R. van Schaijk, J. C. Mann, and J. H. Wolter, *Phys. Rev. B* **56**, 4853 (1997).

¹⁷B. E. Cole, T. Takamasu, K. Takehana, R. Goldhahn, D. Schulze, G. Kido, J. M. Chamberlain, G. Gobsch, M. Henini, and G. Hill, *Physica B* **249**, 607 (1998).

¹⁸J. M. Luttinger and W. Kohn, *Phys. Rev.* **97**, 869 (1955).

¹⁹J. M. Luttinger, *Phys. Rev.* **102**, 1030 (1956).

²⁰D. C. Rogers, J. Singleton, R. J. Nicholas, C. T. Foxon, and K. Woodbridge, *Phys. Rev. B* **34**, 4002 (1986).

- ²¹A. H. MacDonald and D. S. Ritchie, Phys. Rev. B **33**, 8336 (1986).
- ²²G. E. W. Bauer and T. Ando, Phys. Rev. B **37**, 3130 (1988); **38**, 6015 (1988).
- ²³G. Bastard, *Wave Mechanics Applied to Semiconductor Heterostructures* (Les editions de physique, Les Ulis Cedex, France, 1992).
- ²⁴V. B. Timofeev, M. Bayer, A. Forchel, and M. Potemski, Pis'ma Zh. Éksp. Teor. Fiz. **64**, 52 (1996) [JETP Lett. **64**, 60 (1996)].
- ²⁵X. Liu, A. Petrou, A. L. Moretti, F. A. Chambers, and G. P. Devane, Superlattices Microstruct. **4**, 141 (1988).
- ²⁶J. S. Lee, N. Miura, and Y. Iwasa, Surf. Sci. **196**, 534 (1988).
- ²⁷D. Huang, J. I. Chyi, and H. Morkoc, Phys. Rev. B **42**, 5147 (1990).